Mechanical and thermal response of enamel to IR radiation – a Finite Element mesoscopic model

A. Vila Verde, Marta M. D. Ramos*
Departamento de Física, Universidade do Minho, Campus de Gualtar,
4710-057 BRAGA, PORTUGAL

ABSTRACT

We present finite element models of human dental enamel that account for water-pores known to exist in this material, and use them to assess the influence of these pores on the temperature and stress profiles during and after single Er:YAG (2.9 μm) and CO_2 (10.6 μm) laser pulses of duration 0.35 μs. Our results indicate that the temperature maximum is reached at the water-pores at the end of the laser pulse; this maximum seems to be independent of pore size for the CO_2 laser but appears to be strongly dependent of pore size for the Er:YAG laser. The pressure reached at the water pore seems to be directly related to the temperature at the pore and it is significantly higher that the stress levels reached throughout the modelled structure, which indicates that water pores should play a significant role in the ablation mechanisms, even before water vaporization takes place. These results suggest that researchers conducting enamel ablation by Er:YAG lasers - or other lasers with wavelengths for which the absorption coefficients of the mineral and the water differ significantly - may want to select their samples and analyse their results taking into account factors that may alter the degree of mineralization of a tooth, such as age or type of tooth.

Keywords: CO_2 laser, Er:YAG laser, human dental enamel, ablation, mesoscopic modelling, finite element models.

1. INTRODUCTION

Infrared (IR) lasers are already being successfully used for cavity preparation during treatment of dental caries. They are very well accepted by patients because of the reduced pain experienced during treatment, and may present other advantages such as decrease in the concentration of bacteria at the crater surfaces [1]. However, the ablation rates are still low when compared to those obtained with a conventional dental drill, in particular for dental enamel. This characteristic, together with the fact that relatively large quantities of material must be removed to prepare a cavity for filling, implies that conventional cavity preparation using lasers may be significantly more time consuming than using the dental drill.

Lasers like Er:YAG (2.9 μm) or CO_2 (10.6 μm) and others have the potential to do precise dental tissue machining; this potential is not being used to its fullest when employing them to prepare cavities for standard caries treatment. Pearson and co-workers are trying to use this ability to develop a treatment for caries which attempts to minimize the amount of healthy material being removed [2]. The treatment relies on accessing the carious sites through a very narrow tunnel drilled by a laser and using bactericidal substances to kill the cariogenic bacteria in the carious site, instead of removing the diseased tissues as during conventional caries treatment. The potential advantages of this type of treatment relative to conventional caries treatment

* e-mail: marta@fisica.uminho.pt; phone: +351 253 604 330; fax +351 253 678 981; webpage: www.gfct.fisica.uminho.pt.

are many: because the access tunnel is very narrow, the filling material will adhere properly, which will avoid the need to reshape the prepared cavity to ensure the mechanical stability of the filling; for the same reason, the surface area of the access site is small and, consequently, there is less chance of the seal being broken and of bacteria re-entering the site; finally, since the amount of healthy material being removed is much smaller than in conventional caries treatment, the mechanical resistance of the treated tooth is less affected. Ensuring that the chance of re-infection is low and that the mechanical resistance of the tooth is not compromised will have an outstanding impact not only on the health of individuals but also on National Health Systems and on Insurance Dental Health Plans. This impact can be more easily understood if, for example, one remembers that replacement of restorations represents 60% of all the restorative dentistry performed in the United Kingdom [3].

While it is already established that lasers like Er:YAG and CO_2 can be used to ablate dentine and enamel, using them to drill narrow (diameter < 0.5 mm) tunnels implies that the laser operating parameters (pulse duration, pulse repetition, laser intensity, temporal and spatial profile of the laser pulses) still need to be optimized if we are to obtain maximum quality results: maximizing the ablation rates while being able to produce the necessary narrow tunnels with reduced thermal damage like cracks. Optimizing the laser operating parameters is no simple task because of the non-linear nature of ablation. Computational models can play a definitive role here, by allowing us to deepen our understanding of the ablation mechanisms and thus to create a guidance capability that will contribute to finding the best laser operating parameters. In particular, these models must include dentine and enamel's structure and chemical composition at a micrometer and nanometre scale, which is thought to play an important role in ablation. The challenges that must be met in optimizing the ablation of enamel and dentine by IR lasers are similar, but not identical because the structure and composition of those two materials are significantly different. Dental enamel proves to be the most trying material, presenting lower ablation rates and higher risk of fracture because of its higher rigidity and very low water content; consequently, the need for developing good computational models of enamel ablation to provide guidance capability for this procedure is strongly felt.

The enamel models presented here attempt to account for this material's meso-structure by including nanometer-size pores filled with water, which are thought to play a determinant role in the ablation mechanisms. The model was built using the commercial finite element software ABAQUS™ and simulates the thermal and mechanical effects in enamel caused by a single Er:YAG (2.9 μm) or CO_2 (10.6 μm) laser pulse of 0.35 μs duration and sub-ablative intensity. Our aim is to assess the influence of pore size on the stress distribution in enamel during the laser pulse.

2. MODEL DESCRIPTION

Human dental enamel is composed mainly by hydroxyapatite (HA), and also contains small amounts of water and even smaller amounts of organic material. It is known to have a small volume-fraction of pores, but the pore connectivity, volume and area distributions are not known accurately. Still, pores as small as a few tens of nanometres and as large as a few hundreds of nanometres are thought to exist, mostly located in the inter-rod enamel [4]. These pores contain mainly water, but also some organic material.

In order to investigate the effect of pore size on the stress distributions caused by mid-infrared laser pulses, we developed three Finite Element models for enamel (using software ABAQUS™ version 6.4.1) each representing a piece of HA surrounding a single cubic pore containing only water (see Fig. 1). The three models differ only on the size of the pore: the length of the pore edges considered are 30, 70 and 130 nm. The total dimensions of the models are $3.1 \times 3.1 \times 1.29\ \mu m^3$, and they have 49392 nodes and 45374 elements (30 and 70 nm pore models), or 38400 nodes and 31936 elements (130 nm pore model). The models attempt

to represent a small piece of enamel which is a part of a much larger structure (the tooth), so adequate boundary conditions (described below) were used.

Given the small dimensions of the pores, the question that must first be answered is whether the water in the pore will behave like liquid bulk water. The factors that most influence the water behaviour are the pore dimensions and the hydrophilic character of the pore surface: as either of them goes up, the water in a pore will behave closer to liquid bulk water. Work done by Giaya, Liu, Borggreven and co-workers [5-7] strongly suggests that water contained in pores of width larger than 30 nm and pore walls made of HA will behave like liquid bulk water, given that HA is an ionic substance of composition $Ca_{10}^{2+}\left(PO_4^{3-}\right)_6\left(HO^-\right)_2$ and, consequently, can be expected to have a strong hydrophilic character.

The energy of infrared lasers is absorbed by materials and transformed into heat in very fast timescales[8]; consequently, these lasers can be said to have a purely thermal effect on materials, and this is the cause of the mechanical stress that will develop in the material. To assess the thermal effects of two infrared lasers, CO_2 at 10.6 μm and Er:YAG at 2.9 μm, on enamel, we first performed transient heat transfer analysis to obtain the temperature reached at each point (node) of the model, during and after one laser pulse of duration 0.35 μs, for a total time of 10 μs. Subsequently, the temperature distribution was used as input to the dynamic stress simulations, from which we obtained the stress and displacement (distance between the initial and final position of each node) experienced throughout the model. The number of increments for all the analyses was controlled by the automatic incrementation scheme available in ABAQUS™.

2.1 Heat transfer simulations

The transient heat transfer analyses were done using the implicit algorithm in ABAQUS™, taking advantage of user subroutine DFLUX which allowed us to generate heat in each finite element accounting for the spatial and temporal variation of the laser intensity. The intensity of the laser beam inside the tissue at every instant is given by [8]:

$$I(r,z) = I_0.\exp(-\alpha.z).\exp(-2r^2/w^2) \quad (1)$$

where z is the depth inside the tissue, I_0 is the intensity of radiation at the surface of the target and at the centre of the laser spot, α is the absorption coefficient of the tissue, w is the beam radius and r is the radial distance from the centre of the laser spot. We should highlight that the intensity of the laser beam is constant over time, and that no attempt was made to consider the effects of scattering or surface reflectance. The effects of scattering should not be very intense because the absorption coefficients of enamel at the wavelengths considered are high (≈800 cm^{-1}) [9,10] and, therefore, all the radiation is absorbed in the first few micrometers of tissue. The enamel surface reflectance at 10.6 μm is 13% [11] and, since its value at 2.9 μm could not be found in the literature, it was considered zero for both wavelengths. The local heat deposition, S, per unit area and time over a slice of material with thickness Δz is given by

$$S(r,z) = -\frac{\partial I(r,z)}{\partial z} = \alpha.I(r,z) \quad (2)$$

The laser and material parameters used to calculate the heat generated in each element are given in Tables 1 and 3.

Table 1 – Laser parameters

Type of laser	CO_2 (10.6 μm)	Er:YAG (2.94 μm)
Pulse duration (μs)	0.35	0.35
Maximum absorbed intensity, I_0 ($J.m^{-2}.s^{-1}$)	1.2×10^{10}	2×10^{10}
Number of pulses	1	1
Beam radius (mm)	0.2	0.2

Only the specific heat of water is considered to vary with temperature; ABAQUS™ interpolates linearly to obtain values of specific heat for temperatures between those given in Table 3. The absorption coefficients of water (α_{water}) and HA (α_{HA}) in Table 3 were considered constant; a detailed explanation of how they were estimated can be found the work we reported elsewhere [12]. We should note that work by Shori and co-workers [13] indicates that the absorption coefficient for water at $\lambda = 10.6$ μm can be considered constant up to the maximum energy density (energy/volume) reached by water in these simulations. Work by the same authors suggests that, given that the highest energy density reached in the water pore is 0.4 kJ/cm^3, the absorption coefficient of water at $\lambda = 2.9$ μm will decrease from 12 250 cm^{-1} to perhaps 10 000 cm^{-1}, which means that the maximum temperatures calculated by this model will be slightly over-estimated. While the thermal conductivity of water (TC_{water}) varies significantly between room temperature and 150 ºC [14], this will have very little influence on the results because the parameter governing the maximum heat diffusion from the pore is the thermal conductivity of HA (TC_{HA}). The thermal conductivity and the specific heat of HA were considered constant, given that no information otherwise was found in the literature.

The initial temperature of the simulated structure was 37 ºC. Adiabatic boundary conditions were used for all the outside surfaces of the model. These boundary conditions are the most adequate because, in the very short timescale of the simulation, energy transfer into the atmosphere can be considered negligible and, because the temperature gradients across the XY plane are small, heat transfer along that plane is very reduced. In order to simulate the energy losses along OZ, the two bottom layers of elements (named Bottom Restrain-Layer in Fig. 2) were given a higher mass density than HA, thus acting like a heat sink.

2.2 Stress simulations

The dynamic stress-displacement analyses were also performed using ABAQUS™ implicit algorithm. Given that the main material in the pores is water, we decided to approximate the mechanical behaviour of this material by an Equation of State (EOS) for liquid water, which was implemented through user subroutine UMAT. We used the EOS described in the work of Lyons [15], which allows us to obtain the water pressure, P, in the pore at a given temperature, T, and volume per unit mass, V_m:

$$P = B_T \left[\exp\left(-\frac{V_m - V_{0T}}{V_{0T} \times A_T} \right) - 1 \right], \tag{3}$$

where

$$V_{0T} = V_{P0T0}\left(1 + \xi_1 T + \xi_2 T^2 + \xi_3 T^3 + \xi_4 T^4 + \xi_5 T^5\right), \tag{4}$$

$$A_T = A_0\left(1+\eta_1 T+\eta_2 T^2+\eta_3 T^3\right) \text{ and} \quad (5)$$

$$B_T = B_0\left(1+\varsigma_1 T+\varsigma_2 T^2+\varsigma_3 T^3\right). \quad (6)$$

Lyons obtained the values of the constantsV_{P0T0}, A_0, B_0, ξ_i, η_i and ζ_i used in eqs. 3, 4, 5 and 6 by fitting these equations to experimental measurements of temperature, pressure and mass volume for liquid water; the values used in this work can be found in Table 2.

Table 2 – Parameters used for the Equation of State for water.

B_0 (N/m^2)	2.71E+08
A_0	1.38E-01
V_{p0t0} (m^3/kg)	1.00021195720E-03
ξ_1 (ºC^{-1})	-6.10804506610E-05
ξ_2 (ºC^{-2})	8.26422147620E-06
ξ_3 (ºC^{-3})	-6.25191522510E-08
ξ_4 (ºC^{-4})	3.96577772140E-10
ξ_5 (ºC^{-5})	-1.03766115850E-12
η_1 (ºC^{-1})	1.83447912390E-03
η_2 (ºC^{-2})	-3.94832209280E-05
η_3 (ºC^{-3})	1.32756265960E-07
ζ_1 (ºC^{-1})	9.43239862720E-03
ζ_2 (ºC^{-2})	-1.43696702930E-04
ζ_3 (ºC^{-3})	4.56081249050E-07

In UMAT, the volume of the pore at each increment was made a state variable; this quantity is calculated in each increment by taking the volume of the pore in the previous increment and the current strain tensor passed into the subroutine. Having determined the volume of the pore, the stress tensor in the pore can easily be calculated by taking the temperature at the pore and using eqs. 3, 4, 5 and 6: the direct stress components are equal to the pressure calculated using eq. 3, and the shear stress components are zero at every instant.

All the external nodes were fixed in the stress analyses, with the exception of the nodes at the top surface (z = 0), which were left unconstrained. To account for the fact that the simulated structure is under the influence of the rest of the material that constitutes the tooth, the outer layers of elements were given different values of Young's modulus (E) and Poisson's ratio (ν) from those of HA. These outer layers, shown in Fig. 2 (named Bottom Restrain-Layer, with thickness 0.116 μm and Lateral Restrain-Layer, with thickness 0.96 μm), thus make the transition between the fixed nodes and the centre of our model structure. A detailed explanation of how to estimate E and ν for the restrain-layers can be found in our previous work [16].

The number of increments for the stress analyses was controlled by the automatic incrementation scheme available in ABAQUS™.

Table 3 – Material properties

	Hydroxyapatite	Water	Lateral Restrain-layer	Bottom Restrain-layer
Absorption coefficient (cm^{-1})	[10] CO_2: 825 [12] Er:YAG: 300	[10] CO_2: 825 [13] Er:YAG: 12 250	CO_2: 825 Er:YAG: 300	CO_2: 825 Er:YAG: 300
Density at 37ºC ($kg.m^{-3}$)	[17] 3.1×10^3	[18] 9.9×10^2	3.1×10^3	Therm. anal.: 6.2×10^3 Stress anal.: 3.1×10^3
Thermal conductivity ($J.s^{-1}.m^{-1}.ºC^{-1}$)	[19] 1.3	[14] 0.6	1.3	1.3
Specific heat ($J.kg^{-1}.ºC^{-1}$)	[19] 880	[18] 4179, T=313 K 4198, T=353 K 4262, T=403 K 4403, T=453 K 4685, T=503 K 5306, T=553 K	880	880
Young's modulus ($N.m^{-2}$)	[20] 1.1×10^{11}	Not applicable	1.5×10^7	2.89×10^5
Poisson's ratio	[21] 0.28	Not applicable	0.28	0.28
Expansion coefficient ($ºC^{-1}$)	[22] 1.6×10^{-5}	Not applicable	$\alpha_{xx} = 4 \times 10^{-3}$ $\alpha_{yy} = 4 \times 10^{-3}$ $\alpha_{zz} = 1.6 \times 10^{-5}$	0

3. RESULTS AND DISCUSSION

In order to evaluate the effect of the boundary conditions on the stress maps, we used the CO_2 laser parameters and the 70 nm pore model to perform simulations in which the water in the pore was replaced by HA. We compared the results to those previously obtained for the same laser, but using a much larger model ($23 \times 23 \times 35\ \mu m^3$) [16]. The thermal analysis indicates that the maximum temperature (153 ºC) is reached at the irradiated surface, at the end of the laser pulse, and slowly decreases until the end of the simulation, a similar result to the previously published results [16]. Instead of directly comparing stress tensors, we calculated the equivalent Von Mises stress (VMS), a useful quantity to which resort because it combines the nine components of the stress tensor at each element into a single scalar value. We found that the time-averaged VMS levels reached in the current model are significantly higher than but within the same order of magnitude of the ones obtained by us previously with a much larger model [16]. Also, the current results still show an oscillation of the stress values with time, but the period and amplitude of that oscillation differ markedly from the one obtained for a larger model [16]. The maximum VMS values reached concentrate at the end of the laser pulse, for both model sizes. These results suggest that qualitative inferences on the stress behaviour may be made with reasonable confidence from the current results, but the actual values of stress must be interpreted with caution.

Having established the confidence with which the results may be interpreted, we proceeded to perform simulations using the 70 nm pore model and CO_2 laser parameters, but this time considering the water pore to be filled with liquid water. The stress levels at the water pore became one order of magnitude higher than when that region is made of mineral only. As a consequence, the stress levels at the mineral directly surrounding the pore were also elevated. This suggests that the water pores can have a significant

impact in the stress distributions in enamel and can play an important role in ablation, even for relatively low temperature elevations such as the one predicted using the laser parameters in Table 1. It should be noted that the temperatures reached in the material do not allow for water vaporization, because they are always lower than the vaporization temperature at the pressures felt inside the pore. The high pressures in the water pore are solely due to the thermal expansion of the water and the high rigidity of HA, which means that even very small volume variations translate into high mechanical pressures. These results suggest that cracking of enamel may take place even before water-vaporization begins, and that it is possible that vaporization may actually begin only after the pore walls have cracked.

Given that the mechanical properties of HA have such an impact on the stress levels reached at the water pore, and knowing that a biological material like enamel may experience significant changes in its properties depending on its location, we then proceeded to assess the influence of the mechanical properties of HA, E_{HA} and ν_{HA} , on the stress levels reached. Both those parameters were independently varied by ± 10% and ± 25%, using the 70 nm water pore model and CO_2 laser parameters. We found that varying E or ν within the tested range has little effect on the pore pressure: the maximum variation experienced was approximately 3%. Varying E_{HA} has, however, a more pronounced effect on the VMS felt in the mineral directly surrounding the pore: the VMS becomes 15% higher when E_{HA} is raised by 25% and 5% lower when E_{HA} is lowered by 25%. This suggests that different values of E_{HA} will cause some non-intuitive variations on the stress levels experienced throughout enamel, but the general behaviour of the stress remains the same: the higher levels of stress are felt in the pore and in the mineral that surrounds the pore.

We then proceeded to assess the influence of the pore size on the stress levels reached in enamel when using the CO_2 laser, by performing simulations using the 30 and 130 nm pore models. We found that the temperature behaviour was identical to the 70 nm pore model, which was expected because the absorption coefficients of HA and water were considered identical. The pressure at the water pores remained unchanged in all three models, consistent with the identical thermal results in all three models. The time-averaged VMS of the material that directly surrounds the water pore, however, increased significantly (17%) between the 30 nm and the 130 nm model, which was not expected given that the water pressure remained approximately the same in all three models. This result suggests that the size of the water pores by itself influences the stress levels reached by the material, independently of the temperature reached at the pore.

We finally performed simulations using the three geometric models with water pores, but using Er:YAG laser parameters. The temperature distribution at t = 0.35 μs for the 70 nm pore model and the Er:YAG laser can be seen in Fig 1.

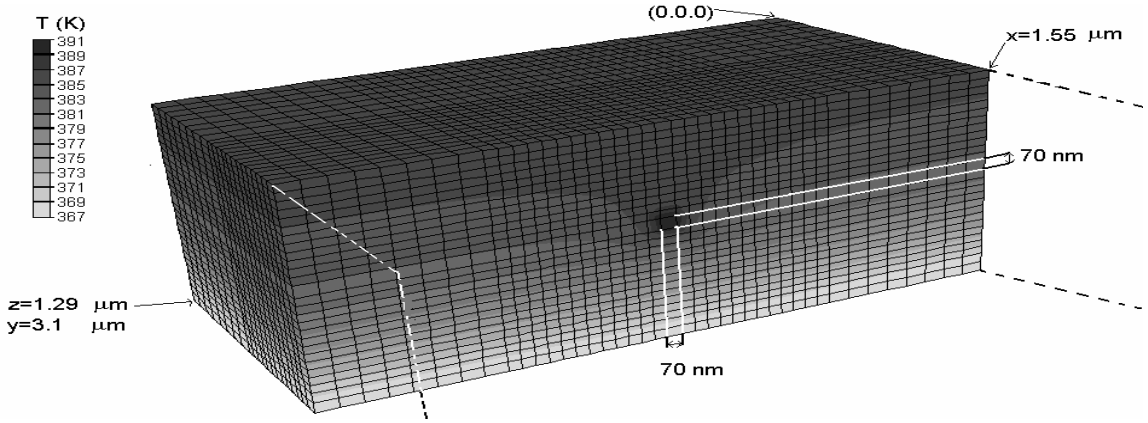

Fig. 1- Temperature map of a piece of HA surrounding a water/organic pore at the end of an Er:YAG laser pulse with the duration of 0.35 μs. The dimensions of the central water/organic pore are $70 \times 70 \times 70$ nm^3. Only half of the structure is shown.

As expected, we found that the water pore was the site with the highest temperature in each model, because of the difference in the absorption coefficients of water and HA. We also found that the maximum temperature reached at the water pore (at the end of the laser pulse) is a strong function of the pore size for Er:YAG, as can be seen in Table 4. This can easily be explained if we remember that smaller pores have higher area-to-volume ratios and, therefore, lose heat to their surroundings more rapidly than larger pores. One microsecond after the laser pulse, the pore reaches thermal equilibrium with its surroundings and the temperature in all three models is 106 ºC. The actual temperature values should not be considered entirely accurate because of the uncertainty associated with the material parameters used, in particular the absorption coefficient of water at $\lambda = 2.9$ μm, as discussed in section 2. However, since the minimum value that α_{water} can reach is 10 000 cm^{-1} (according to work by Shori et al. [13]) which is still significantly higher than α_{HA} (300 cm^{-1}), we can confidently say that our results provide insight into the processes taking place.

Consistent with the temperature maps obtained for Er:YAG laser parameters, the stress maps (see Fig. 2 for an example) indicate that the water pores reach a maximum pressure at the end of the laser pulse, and this maximum pressure varies significantly with pore size, as can be seen in Table 4: there is a 50% increase in peak-pressure from the 30 nm to the 130 nm pore models. This is most likely a consequence not only of the increase in pore size, but also of the increase in the pore peak-temperature. The time averaged pore-pressure and time-averaged VMS throughout all the models also increase as the pore size increases.

Table 4- Maximum temperature and pressure reached at the pores for all the models.

	Er:YAG		CO_2	
Pore dimensions (nm^3)	Maximum temperature (ºC)	Maximum pressure (N/m^2)	Maximum temperature (ºC)	Maximum pressure (N/m^2)
$30 \times 30 \times 30$	110	9.0e7	153	1.6e8
$70 \times 70 \times 70$	118	1.0e8	153	1.6e8
$130 \times 130 \times 130$	135	1.4e8	153	1.6e8

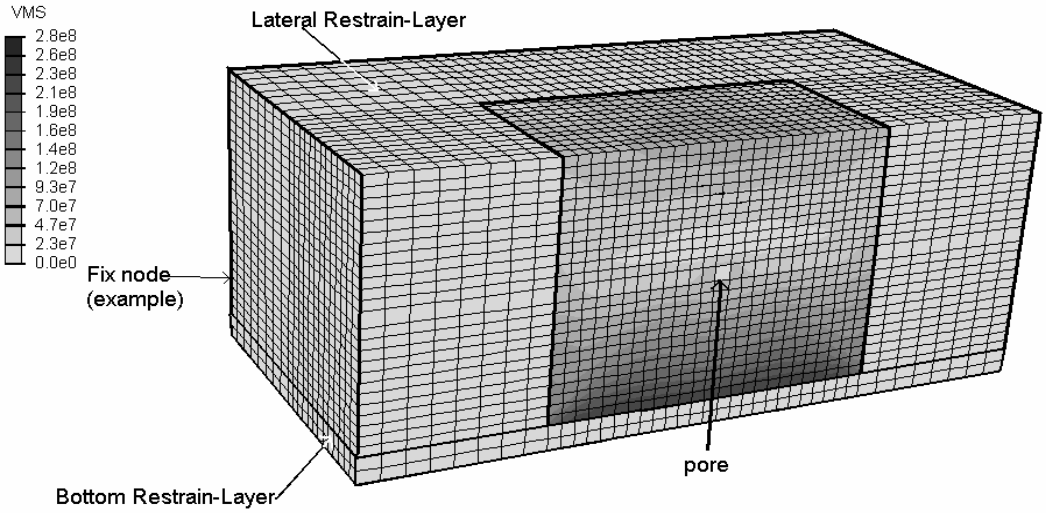

Fig. 2-Von Mises stress (N/m^2) at t = 0.44 μs for the 70 nm pore model with Er:YAG laser. Only half of the model is shown.

Comparing the results from equally-sized pore models and different lasers, we find that in all situations the maximum and the time-averaged VMS, and the corresponding maximum and time averaged pore pressure are always higher for the CO_2 laser. This is consistent with the fact that, for the chosen laser intensities, this laser caused significantly higher temperature rises (both peak and long-term) than Er:YAG, that is, the total energy-per-unit-mass deposited by the CO_2 laser was larger than by the Er:YAG laser. These results suggest that, if we select CO_2 and Er:YAG laser intensities that allow us to deposit the same total energy-per-unit-mass in the material, the pore peak-temperature at the end of the laser pulse may be significantly higher when using the Er:YAG laser; in these conditions, a much higher peak stress may develop when using this laser instead of the CO_2 laser, which means that, for the same total energy-per-unit-mass deposited using both lasers, ablation may begin with the Er:YAG laser but not with the CO_2 laser. This is consistent with experimental data indicating that Er:YAG ablation cause lower thermal damage than ablation by CO_2 lasers.

4. CONCLUSIONS

Our results strongly suggest that the temperature reached by the water pores is a function of pore size for Er:YAG radiation, and is much less dependent of pore size for CO_2 radiation. Since the results also indicate that the pressure reached inside the water pores is directly related to the water temperature and also to the pore size by itself, it follows that the pressure distribution may be very dependent of the pore-size distribution for Er:YAG lasers and less so for CO_2 lasers. We found that very high pressures can be reached even in the absence of vaporization, caused simply by the thermal expansion of the liquid water: while water expands only a few percent when temperature rises by 100ºC, the fact that HA has a high Young's modulus means that even small volume variations will translate into very high water pressures. While the actual stress values described in this work must be interpreted with caution, the results seem to indicate that cracking of enamel may occur even in the absence of water vaporization, and that water vaporization may begin only after the walls of pores have been damaged by cracks.

Results also suggest that the onset of cracking may be reached by Er:YAG lasers using lower absorbed fluences than by CO_2 lasers because, for the same amount of deposited energy, the Er:YAG lasers will cause a higher temperature peak and, consequently, a higher pressure peak, at the water pores than the CO_2 lasers. Nevertheless, given the variability in pore size that must be expected in a biological material like enamel, our results indicate that the enamel ablation threshold by Er:YAG lasers may be harder to predict and reproduce than by CO_2 lasers, because the maximum pressure reached at the pores seems to be very dependent of pore size for Er:YAG, but less so for CO_2 lasers. This may explain the fact that the threshold ablation fluences for enamel by Er:YAG lasers seem to be more variable than for CO_2; so much so that finding threshold ablation fluences for enamel irradated with Er:YAG lasers in the literature is significantly more difficult than for CO_2 lasers.

More generally, these results suggest that researchers may want to select their tooth samples and interpret their results taking in consideration factors that may influence the degree of mineralization and, consequently, the pore size distribution, such as age or even region of the tooth, especially when using laser wavelengths known to be absorbed differently by the different components of enamel.

ACKNOWLEDGEMENTS

This work was approved by the Portuguese Foundation for Science and Technology, FCT, and POCTI, and supported by the European Community Fund FEDER under project no.

POCTI/ESP/37944/2001. One of us (A.V.V.) is also indebted to FCT for financial support under PhD grant no. SFRH/BD/4725/2001 and thanks Mr. Richard Kramer Campen, at Penn State University and Prof. Marshall Stoneham, at University College London, for helpful discussions during the course of this work.

REFERENCES

1. D. M. Harris and M. Yessik. "Therapeutic Ratio Quantifies Laser Antisepsis: Ablation of Porphyromonas gingivalis With Dental Lasers." Lasers in Surgery and Medicine, **35**, 206-213, 2004.

2. S. Bowe. "An investigation into Er:YAG laser ablation of enamel", (MSc thesis), Eastman Dental Institute, University of London (1999).

3. "Effective health care: Dental restoration: what type of filling?" University of York - NHS Centre for Reviews and Dissemination, York, (1999).

4. G. H. Dibdin and D. F. G. Poole. "Surface-area and pore-size analysis for human-enamel and dentine by water-vapor sorption." Archives of Oral Biology, **27**, 235-241, 1982.

5. A. Giaya and R. W. Thompson. "Water confined in cylindrical micropores." Journal of Chemical Physics, **117**, 3464-3475, 2002.

6. Y.-C. Liu, Q. Wang and L.-H. Lu. "Water confined in nanopores: its molecular distribution and diffusion at lower density." Chemical Physics Letters, **381**, 210-215, 2003.

7. J. M. P. M. Borggreven, F. C. M. Driessens and J. W. E. Vandijk. "Diffusion through bovine tooth enamel as related to the water- structure in its pores." Archives of Oral Biology, **25**, 345-348, 1980.

8. H. M. Niemz. "Laser-Tissue Interactions - Fundamentals and applications", Springer-Verlag, Berlin, 1996.

9. D. Fried, M. J. Zuerlein, J. Featherstone, W. Seka, C. Duhn and S. M. McCormack. "IR laser ablation of dental enamel: mechanistic dependance on the primary absorber." Applied Surface Science, **127-129**, 852-856, 1998.

10. M. J. Zuerlein, D. Fried, J. D. B. Featherstone and W. Seka. "Optical properties of dental enamel in the mid-IR determined by pulsed photothermal radiometry." Ieee Journal of Selected Topics in Quantum Electronics, **5**, 1083-1089, 1999.

11. D. Fried, R. E. Glena, J. D. B. Featherstone and W. Seka. "Permanent and transient changes in the reflectance of CO_2 laser-irradiated dental hard tissues at λ=9.3, 9.6, 10.3, and 10.6 μm and at fluences of 1-20 J/cm^2." Lasers in Surgery and Medicine, **20**, 22-31, 1997 (132).

12. A. Vila Verde, M. M. D. Ramos, A. M. Stoneham and R. M. Ribeiro. "Mesoscopic modelling of the interaction of infrared lasers with composite materials: an application to human dental enamel." Applied Surface Science, **238**, 410-414, 2004.

13. R. K. Shori, A. A. Walston, O. M. Stafsudd, D. Fried and J. T. Walsh. "Quantification and modeling of the dynamic changes in the absorption coefficient of water at λ=2.94 μm." Ieee Journal of Selected Topics in Quantum Electronics, **7**, 959-970, 2001.

14. G. V. Samsonov (ed.) "The oxide handbook", IFI/Plenum, New York, USA, 1982.

15. C. G. Lyons. "Simple equation of state for dense fluids." Journal of Molecular Liquids, **69**, 269-281, 1996.

16. A. Vila Verde and M. M. D. Ramos. "Boundary conditions for 3-d dynamic models of ablation of ceramics by pulsed mid-infrared lasers." Applied Surface Science, **in print**, 2004.

17. "American Mineralogist", 74, pp 870, Mineralogical Society of America, 1989 (quoted in euromin.w3sites.net//mineraux/HYDROXYLAPATITE.html).

18. J. R. Cooper and E. J. Le Fevre. "Thermophysical properties of water substance - Student's tables in SI units", Edward Arnold Ltd, London, 1975.

19. H. H. Moroi, K. Okimoto, R. Moroi and Y. Terada. " Numeric approach to the biomechanical analysis of thermal effects in coated implants." International Journal of Prosthodontics, **6**, 564-572, 1993 (quoted in 'Dental Tables' at http://www.lib.umich.edu/).

20. M. Braden. "Biophysics of the tooth". in "Physiology of Oral Tissues", Vol. 2 (ed. Y. Kawamura), pp. 1-37, S. Karger AG, Basel, 1976.

21. D. E. Grenoble, J. L. Katz, K. L. Dunn, R. S. Gilmore and K. L. Murty. "The elastic properties of hard tissues and apatites." Journal of biomedical materials research, **6**, 221-223, 1972 (291).

22. J. Czernuszka. "Hydroxyapatite". in "The encyclopedia of advanced materials", Vol. 4 (eds. D. Bloor, M. C. Flemings, R. Brook, S. Mahajan and R. Cahn), pp. 1076, Elsevier Science Ltd, Cambridge, Great Britain, 1994.